



HAL
open science

Design of auxiliary systems for spectroscopy

Marco Vanzini, Francesco Sottile, Igor Reshetnyak, Sergio Ciuchi, Lucia Reining, Matteo Gatti

► **To cite this version:**

Marco Vanzini, Francesco Sottile, Igor Reshetnyak, Sergio Ciuchi, Lucia Reining, et al.. Design of auxiliary systems for spectroscopy. Faraday Discussions, 2020, 10.1039/D0FD00067A . hal-02996427

HAL Id: hal-02996427

<https://hal.science/hal-02996427>

Submitted on 10 Nov 2020

HAL is a multi-disciplinary open access archive for the deposit and dissemination of scientific research documents, whether they are published or not. The documents may come from teaching and research institutions in France or abroad, or from public or private research centers.

L'archive ouverte pluridisciplinaire **HAL**, est destinée au dépôt et à la diffusion de documents scientifiques de niveau recherche, publiés ou non, émanant des établissements d'enseignement et de recherche français ou étrangers, des laboratoires publics ou privés.

Cite this: DOI: 00.0000/xxxxxxxxxx

Design of auxiliary systems for spectroscopy

Marco Vanzini^{a,b,c}, Francesco Sottile^{a,b}, Igor Reshetnyak^d, Sergio Ciuchi^{e,f}, Lucia Reining^{a,b} and Matteo Gatti^{a,b,g}

Received Date

Accepted Date

DOI: 00.0000/xxxxxxxxxx

The Kohn-Sham system is the prototypical example of an auxiliary system that targets, in principle exactly, an observable like the electronic density without the need to calculate the complicated many-body wavefunction. Although the Kohn-Sham system does not describe excited-state properties directly, it represents a very successful strategy guideline also for many spectroscopy applications. Here we propose a generalization of the Kohn-Sham idea. In many situations one is interested only in limited answers to specific questions, whereas in state-of-the-art approaches a lot of information is generally calculated that is not needed for the interpretation of experimental spectra. For example, while the target is a spectrum $S(\omega)$ like the optical absorption of a solid, within time-dependent density-functional theory (TDDFT) one calculates the whole response function $\chi(\mathbf{r}, \mathbf{r}', \omega)$. Analogously, within many-body perturbation theory (MBPT) one calculates the whole one-particle Green's function $G(\mathbf{r}, \mathbf{r}', \omega)$, while only the total spectral function $A(\omega)$ is needed for angle-integrated photoemission spectra. In this contribution, we advocate the possibility to design auxiliary systems with effective potentials or kernels that target only the specific spectral properties of interest and are simpler than the self-energy of MBPT or the exchange-correlation kernel of TDDFT. In particular, we discuss the fundamentals and prototypical applications of simplified effective kernels for optical absorption and spectral potentials for photoemission, and we discuss how to express these potentials or kernels as functionals of the density.

1 Introduction

In all spectroscopy experiments one perturbs a sample with an external mean (e.g. a beam of photons, electrons or neutrons) driving the system into an excited state^{1,2}. If the external perturbation is not too strong (so that the sample is not modified during the experiment), the measurement of the system response gives access to the elementary excitations that characterize the physical properties of the material^{3,4}. The measured spectra are affected both quantitatively and qualitatively by the electron-electron interaction⁵, which poses a challenge for their interpretation or prediction. Features such as finite quasiparticle linewidths and satellites in photoemission spectra⁶, bound excitons^{7,8} and double excitations⁹ in optical spectra, or double plasmons^{10,11} in loss spec-

tra, are all signatures of the Coulomb interaction that cannot be captured within an independent-particle picture. Apparently, the theoretical description and analysis of excitation spectra hence require the solution of a complex many-body problem.

However, each spectrum contains only a limited amount of information and each spectroscopy probes a different kind of excitation: for example, electron removal and addition excitations in photoemission or neutral electron-hole excitations in absorption spectroscopy¹. Indeed, observables are formally obtained as expectation values of the many-body wavefunction through high-dimensional integrals, implying that most of the detailed information carried by the wavefunction itself is actually not required¹². We can thus wonder: Is it possible to bypass the many-body problem of the calculation of the wavefunction and obtain directly the quantity of interest?

The Kohn-Sham approach¹³ to density-functional theory¹⁴ (DFT), together with its extension to the time-dependent case within time-dependent density-functional theory¹⁵ (TDDFT), shows that a positive answer to this question indeed exists, at least for the electronic density $n(\mathbf{r}, t)$. The Kohn-Sham scheme represents the prominent example of an auxiliary system of fictitious electrons subjected to an effective potential: the local and real potential $v_{\text{KS}}(\mathbf{r}, t)$, which besides the original external potential also contains Hartree and exchange-correlation (xc) contri-

^a Laboratoire des Solides Irradiés, École Polytechnique, CNRS, CEA/DRF/IRAMIS, Institut Polytechnique de Paris, F-91128 Palaiseau, France.

^b European Theoretical Spectroscopy Facility (ETSF).

^c Theory and Simulation of Materials (THEOS), École Polytechnique Fédérale de Lausanne, CH-1015 Lausanne, Switzerland.

^d Chaire de Simulation à l'Échelle Atomique (CSEA), École Polytechnique Fédérale de Lausanne (EPFL), CH-1015 Lausanne, Switzerland.

^e Dipartimento di Scienze Fisiche e Chimiche, Università dell'Aquila, via Vetoio, I-67010 Coppito-L'Aquila, Italy.

^f Istituto dei Sistemi Complessi-CNR, Via dei Taurini 19, I-00185 Rome, Italy.

^g Synchrotron SOLEIL, L'Orme des Merisiers, Saint-Aubin, BP 48, F-91192 Gif-sur-Yvette, France.

butions. The effective Hamiltonian is much simpler to solve than the initial one: the Kohn-Sham electrons are non-interacting*, giving rise to a single-particle Hamiltonian. The only requirement of the Kohn-Sham auxiliary system is to yield the same density $n(\mathbf{r},t)$ as the original interacting electron system. Instead, for example, the many-body Kohn-Sham wavefunction is a Slater determinant and its single-particle density matrix is idempotent (i.e., occupation numbers are either 0 or 1): both are thus inherently different from the corresponding quantities that are obtained from the full solution of the many-body Hamiltonian. The Kohn-Sham potential of (TD)DFT can be understood as a mean field made exact uniquely for the target quantity, $n(\mathbf{r},t)$. Within many-body perturbation theory^{5,18} (MBPT), the role of the self-energy $\Sigma_{xc}(\mathbf{r}_1, \mathbf{r}_2, \omega)$ can also be interpreted in a similar manner. As a matter of fact, the self-energy is the effective operator describing exchange-correlation effects that yields the single-particle Green's function $G(\mathbf{r}_1, \mathbf{r}_2, \omega)$, without the need of knowing explicitly multi-particle excitations contained in the many-body wavefunction or in Green's functions of higher orders. In contrast to the Kohn-Sham potential, the self-energy is spatially non-local: already the first-order term of the perturbation expansion in the Coulomb interaction contains the non-local Fock exchange operator; frequency dependent: dynamical correlation effects beyond Hartree-Fock give rise to the renormalization of quasiparticles and additional structures in the spectra such as satellites; complex: its imaginary part describes the finite lifetime of quasiparticles and is responsible for the band-gap opening in Mott insulators⁵.

The definition of auxiliary systems seems a very appealing strategy also to obtain excitation spectra circumventing the many-body problem. Ref.¹⁹ showed that generalizations of the Kohn-Sham auxiliary system are indeed possible also for spectral quantities. In particular, the suggestion of a local, real, yet dynamical, spectral potential $v_{\text{SF}}(\mathbf{r}, \omega)$ for photoemission has been later investigated more in detail for exactly solvable models^{20,21} and prototypical materials²². The spectral potential has a much simpler form than the self-energy. Even though it is real, through its frequency dependence it is still constructed to reproduce, in principle exactly, all features associated to the imaginary part of the self-energy.

How far can we extend this idea to spectroscopy? If we target frequency-dependent excitation spectra only, which are the simplest auxiliary systems that are peculiar to each spectroscopy? Are the corresponding effective potentials pathological or are they still amenable to approximations guided by physical ideas? In the rest of the article we explore some answers to those questions: After having outlined the general problem in Sec. 2, in Secs. 3 and 4 we examine the specific cases of angle-integrated photoemission and absorption spectroscopy, respectively, with numerical results for prototypical materials. Finally, we summarize our conclusions in Sec. 5.

* In general, one can devise auxiliary particles whose other physical properties may be different from real electrons as well, see e.g. Refs.^{16,17}.

2 General framework

We aim to calculate a generic excitation spectrum $S(\omega)$ of a many-electron system. At the same time we suppose to be able to determine the spectrum $S_0(\omega)$, typically the one corresponding to the original Hamiltonian without electron-electron interaction, or for a model or a material that is solvable with high accuracy (possibly exactly). Spectra are generally a part of the information carried by correlation functions^{19,23}, which we formally indicate as $S(\omega) = p\{C(\omega)\}$ and $S_0(\omega) = p\{C_0(\omega)\}$.[†] A way to connect the two spectra is to introduce a Dyson-like equation between them, which, focusing on frequency-dependent spectra, can be schematically written as:

$$C(\omega) = C_0(\omega) + C_0(\omega)K(\omega)C(\omega) \quad (1)$$

or, if the inverse functions exist in a common domain, equivalently:

$$K(\omega) = C_0^{-1}(\omega) - C^{-1}(\omega). \quad (2)$$

The issue of determining $S(\omega)$ is therefore translated into the calculation of the kernel $K(\omega)$ of the Dyson equation. The advantage of the structure of Dyson equations is that low-accuracy approximations to $K(\omega)$ can give spectra $S(\omega)$ of higher accuracy than equivalent direct approximations to $S(\omega)$. Therefore one usually can find Dyson equations in many different contexts, from MBPT and TDDFT to dynamical mean-field theory²⁴ (DMFT).

$K(\omega)$ (which can be alternatively named 'kernel' or 'potential'[‡]) defines the auxiliary system that is designed to give the specific target $S(\omega)$, but not other spectra. So, for each spectroscopy, one has to introduce a different auxiliary system. Since the target here is a frequency-dependent function $S(\omega)$ and not a space-dependent quantity like the density $n(\mathbf{r})$, the simplest possible *ansatz* is a frequency-dependent $K(\omega)$, so even simpler than the Kohn-Sham potential $v_{\text{KS}}(\mathbf{r})$ of DFT or the spectral potential $v_{\text{SF}}(\mathbf{r}, \omega)$ for photoemission.

The obvious question is that a new auxiliary system becomes useful only if it is possible to obtain a satisfactory approximation for its effective potential (or kernel) $K(\omega)$. One can expect that working with more compact objects can make their approximation harder to find. Different strategies of approximation have been followed in the various contexts. Within MBPT, diagrammatic techniques combined with physical intuition of fundamental processes have been often the guide to find successful approximations^{5,25}, while in the context of DFT exact constraints or fits of semi-empirical parameters in large sets of compounds have been also often employed (see e.g. Refs.²⁶⁻³⁵).

A very popular route, especially within DFT and its extensions, is to build an accurate knowledge of the effective potential in a model and import this information into the systems under study

† Analogously, the density is also a part of the Green's function, its diagonal: $n(\mathbf{r},t) = -iG(\mathbf{r}, \mathbf{r}, t, t^+)$.

‡ Correlation functions are generally complex functions, so $K(\omega)$ is generally complex as well. However, static and real potentials, like the Kohn-Sham potential, are also possible. In Sec. 3 we will discuss an effective potential that is real, while in Sec. 4 we will investigate an effective kernel that is complex.

through a proper prescription. Notably, the local density approximation¹³ (LDA) chooses the homogeneous electron gas (HEG) as the model system: its xc potential³⁶ is used in real materials through their local electronic density. Recently, in Ref.³⁷ this approach has been turned into a general formal strategy, called the “connector theory”. Along this line, in Sec. 3 we will explore the possibility to extract information from the HEG for a new auxiliary potential $v_{\text{pes}}(\omega)$ that directly targets angle-integrated spectral functions.

In the following, we will also exploit the fact that $S(\omega)$ is often a part of the information contained in more complex correlation functions. In these cases $K(\omega)$ can be expressed in terms of those quantities and successful approximations can be found. The representative example of this strategy is the Sham-Schlüter equation^{38,39} of DFT, which can be also used to devise approximations within optimized effective potential⁴⁰ schemes. In Sec. 4 we will revisit the TDDFT Nanoquanta kernel^{19,41–46} from this perspective, and we will introduce auxiliary systems with frequency-dependent kernels $f^{\text{abs}}(\omega)$ that are even more compact than TDDFT for the calculation of optical spectra.

3 Photoemission spectroscopy

3.1 Spectral function: state of the art

By measuring the one-electron addition and removal energies, angle-resolved photoemission spectroscopy (ARPES) is one of the most direct ways to probe the electronic structure of a material^{6,47}. If one ignores many subtleties related to the photoemission process itself⁴⁸, ARPES spectra can be interpreted within the sudden approximation in terms of the \mathbf{k} -dependent spectral function:

$$A(\mathbf{k}, \omega) = \frac{1}{\pi} |\text{Im}G(\mathbf{k}, \omega)|, \quad (3)$$

where the one-particle Green’s function[§] $G(\mathbf{k}, \omega)$ can be calculated from the Dyson equation^{5,18}:

$$G^{-1}(\mathbf{k}, \omega) = G_H^{-1}(\mathbf{k}, \omega) - \Sigma_{\text{xc}}(\mathbf{k}, \omega). \quad (4)$$

Here G_H is the Green’s function associated to the Hartree hamiltonian and the self-energy Σ_{xc} describes all the many-body exchange-correlation effects. Within Kohn-Sham DFT, the complex and non-local self-energy is replaced by the real and local xc potential v_{xc} , which is however not meant to give the correct spectral function $A(\mathbf{k}, \omega)$. The infamous “band-gap problem” of Kohn-Sham DFT is a manifestation of this issue^{38,49}. Various approximations to the self-energy Σ_{xc} , with different ranges of validity, are today very popular, ranging from Hedin’s GW approximation (GWA)⁴⁸ of MBPT to DMFT in the single site approximation²⁴. Both in the GWA and DMFT approximations, the self-energy has a non-zero imaginary part, leading to effects and satellites due to the electron-electron interaction. In the following we will instead restrict our focus to real and non-local DFT hybrid functionals, such as the Heyd-Scuseria-Ernzerhof HSE06 functional^{50,51}. They can be considered as static approximations to $\Sigma_{\text{xc}}(\mathbf{k}, \omega)$ giving satisfactory results for quasi-particle energies in a large set of

sp semiconductors and metals (see e.g. Refs.^{52–55}).

All the computational schemes that make use of approximate non-local and/or dynamical self-energies, including hybrid functionals, are intrinsically more expensive than the Kohn-Sham DFT approach with a local potential. The search for alternative shortcuts is thus a very active field of investigation.

3.2 Effective potentials for photoemission

In Ref.¹⁹ it was shown that the auxiliary system determined by the spectral potential $v_{\text{SF}}(\mathbf{r}, \omega)$ is capable to yield, in principle exactly, the local spectral function

$$A(\mathbf{r}, \omega) = \frac{1}{\pi} |\text{Im}G(\mathbf{r}, \mathbf{r}, \omega)|, \quad (5)$$

together with all the observables that can be derived from it, such as the electron density:

$$n(\mathbf{r}) = \int_{-\infty}^{\mu} d\omega A(\mathbf{r}, \omega) \quad (6)$$

(with μ the Fermi energy), and the total spectral function $A(\omega)$ measured by angle-integrated photoemission (PES)⁴⁷:

$$A(\omega) = \frac{1}{\pi} \int d\mathbf{r} |\text{Im}G(\mathbf{r}, \mathbf{r}, \omega)| = \frac{1}{\pi} \int \frac{d\mathbf{k}}{8\pi^3} |\text{Im}G(\mathbf{k}, \omega)|. \quad (7)$$

The auxiliary system with the spectral potential $v_{\text{SF}}(\mathbf{r}, \omega)$ represents already a significant simplification with respect to approaches based on the self-energy $\Sigma_{\text{xc}}(\mathbf{r}, \mathbf{r}', \omega)$. However, if one is interested *only* in a frequency-dependent excitation spectrum like $A(\omega)$, it is also conceivable to look for further simplifications.

Therefore, we consider here the idea of a purely frequency-dependent and real effective potential $v_{\text{pes}}(\omega)$. In contrast to the local spectral potential $v_{\text{SF}}(\mathbf{r}, \omega)$, $v_{\text{pes}}(\omega)$ is a number in any basis. $v_{\text{pes}}(\omega)$ has to connect the spectral function $A_0(\omega)$ that is known in some approximation with the target $A(\omega)$. For simplicity, we assume that the Hamiltonian that gives rise to $A_0(\omega)$ is real and static. In such a case, the spectral function associated to $v_{\text{pes}}(\omega)$ is simply $A_{\text{pes}}(\omega) = A_0(\omega - v_{\text{pes}}(\omega))$. If the range of $A(\omega)$, namely the set of values of $A(\omega)$ for varying ω , is a subset of the range of $A_0(\omega)$, the effective potential $v_{\text{pes}}(\omega)$ can be defined on the same frequency domain such that:

$$A(\omega) = A_{\text{pes}}(\omega) = A_0(\omega - v_{\text{pes}}(\omega)). \quad (8)$$

This amounts to looking for the frequency $\tilde{\omega} = \omega - v_{\text{pes}}(\omega)$ such that $A_{\text{pes}}(\omega) = A(\omega) = A_0(\tilde{\omega})$.

In the next sections we will use Eq. (8) to perform a reverse-engineering study and determine $v_{\text{pes}}(\omega)$ for three prototypical solids: sodium, aluminum and silicon. On the basis of this analysis, we will then suggest a route for possible constructive approximations.

3.3 Dependence on the choice of the spectral function A_0

For each material, we fix a target spectral function $A = A_{\text{target}}$ for which we adopt the HSE06 functional as a cheap, but realistic descriptor of the electronic structure of the three materials. In all panels of Figs. 1, 2, 3, for sodium, aluminum and silicon, respec-

§ Here and in the following all quantities are defined at T=0 K.

tively, the blue lines are the target HSE06 spectral functions.

We first examine the starting-point dependence of v_{pes} . According to the choice of the approximated spectral function A_0 in Eq. (8), a different v_{pes} is required to give the same target $A(\omega)$. We consider two different spectral functions A_0 , namely the Hartree approximation or the LDA. In Figs. 1, 2, 3, the green lines are the starting spectral functions A_0 , corresponding to the Hartree approximation in the left panels and the LDA in the right panels of each figure.

In each case, we numerically invert the equation

$$A(\omega) = A_0(\omega - v_{\text{pes}}(\omega)) \quad (9)$$

to determine the potential $v_{\text{pes}}(\omega)$ that sends $A_0(\omega) \rightarrow A(\omega)$. The result is represented in each panel of Figs. 1, 2, 3 by the red plot. For each frequency ω many solutions of the inversion are possible, since for a given value of A , there are usually several frequencies at which $A_0 = A$. However, it is often possible to identify a particular solution by inspecting the two spectral functions and connecting corresponding features (e.g., the band bottom of A with the band bottom of A_0). In such a way, with respect to the raw potential, which is a mere collection of points, we can distillate a function of ω , however discontinuous, which we call the *physical* potential $v_{\text{pes}}(\omega)$. In particular, this physical potential emerges (notably after 10 eV in sodium, or after 25 eV in aluminum) as the (almost) flat line that represents the center of gravity of the other solutions that are instead always scattered on a wide range. As expected, in these cases we find that the closer is the starting point to the target spectral function, the smaller is this physical potential. Whenever an important structure appears in the target spectral functions, like a dip as for aluminum or the gap for silicon, the physical potential $v_{\text{pes}}(\omega)$ has to undergo wild oscillations. These sudden variations of $v_{\text{pes}}(\omega)$ are larger for the left panels compared to the right panels, as the Hartree spectral function is farther from the HSE06 target than the LDA. This is most evident for the band gap region of silicon (around 0 eV), where in the Hartree case the only possible solution undergoes a large jump (until ~ 12 eV), while for the LDA there is also another solution at ~ 0 eV that does not require such a large oscillation. We can therefore conclude that $v_{\text{pes}}(\omega)$ seems more amenable to a simple approximation if one considers the LDA as the starting point rather than the Hartree approximation. We will examine this possibility more closely in the next section.

3.4 A path for approximations

A great share of the popularity of the Kohn-Sham scheme in DFT derives from the fact that the xc potential $v_{\text{xc}}(\mathbf{r})$ has been accurately calculated once and for all in the HEG³⁶ and that simple prescriptions like the LDA are available for its use in inhomogeneous materials. A similar approach has been investigated recently also for the dynamical local spectral potential $v_{\text{SF}}(\mathbf{r}, \omega)$ in Ref.²². So it appears sensible to explore the same path also in the present case for the scalar potential $v_{\text{pes}}(\omega)$.

Also in the HEG, for each density n^h , we can establish a relation

analogous to Eq. (8):

$$A^h(\omega) = A_0^h(\omega - v_{\text{pes}}^h(\omega)) \quad (10)$$

where $v_{\text{pes}}^h(\omega)$ is the scalar potential that in the HEG allows one to obtain $A^h(\omega)$ from $A_0^h(\omega)$. The great advantage of the HEG as a model is that, besides being a universal limit of all extended systems, all the spectral functions considered here are monotonic functions of frequency and hence uniquely invertible: as a consequence, the potential $v_{\text{pes}}^h(\omega)$ is a smooth function of ω .

Following the connector theory³⁷, one should look for a prescription that for each frequency associates the effective potential $v_{\text{pes}}(\omega)$ to the HEG $v_{\text{pes}}^h(\omega)$ with a different density n^h :

$$v_{\text{pes}}(\omega) = v_{\text{pes}|n^h=\mathcal{F}(\omega, [n])}^h(\omega). \quad (11)$$

If the two functions span the same range of values, there exists in principle at least one exact connector³⁷ $n^h = \mathcal{F}(\omega, [n])$.

Here we consider the simplest possible connector approximation that is obtained by setting for all frequencies n^h equal to the average density \bar{n} of each material and by aligning the frequency axes in such a way that $v_{\text{pes}}(\omega + \mu) = v_{\text{pes}|n^h=\bar{n}}^h(\omega + \mu^h)$, so that at $\omega = 0$ both sides refer to their Fermi energy. This gives:

$$v_{\text{pes}}(\omega) = v_{\text{pes}|n^h=\bar{n}}^h(\omega - \mu + \mu^h). \quad (12)$$

We examine this approximation for the three prototypical materials. As in Sec. 3.3, the scalar potential is meant to send the spectral function A_0 (either Hartree or LDA) into the target HSE06 spectral functions. In all cases, we observe that the approximation (12) gives already a good estimation (see purple lines in Figs. 1, 2, 3) of the effective potential v_{pes} obtained directly from the inversion of Eq. (9). The agreement between the potential imported from the HEG and one reference solution (what we called the physical potential in Sec. 3.3) is almost perfect for sodium (Fig. 1), as expected since sodium is very close to the HEG, and also for aluminum (Fig. 2). It remains good even for the onset of the valence band of silicon (Fig. 3), but it degrades towards the band gap region, where a more elaborate connector would be needed. In any case, as discussed in Sec. 3.3, the LDA is a better starting point than the Hartree approximation as $v_{\text{pes}}(\omega)$ can more easily be approximated by $v_{\text{pes}}^h(\omega)$, even in the region of the gap of silicon.

We can now test this possibility in practice, and use $v_{\text{pes}}^h(\omega)$ to calculate the spectral function from Eq. (9), to be compared with our target spectral function. If the results are promising, this would open interesting perspectives, since such an approach requires only 1) a low-effort starting-point spectral function A_0 , 2) a frequency-dependent scalar potential in the HEG, which can be evaluated once and for all for different values of densities and then tabulated, and 3) the chemical potential μ to set up the connector. Thanks to this procedure, the calculation and the use of the HSE06 non-local potential, which is computationally the most demanding part of a standard calculation, is completely bypassed.

The results are shown in Figs. 4 and 5. For the two metals, there is hardly a difference in starting from Hartree or from the LDA. The overall shape is an exceptionally good approximation to

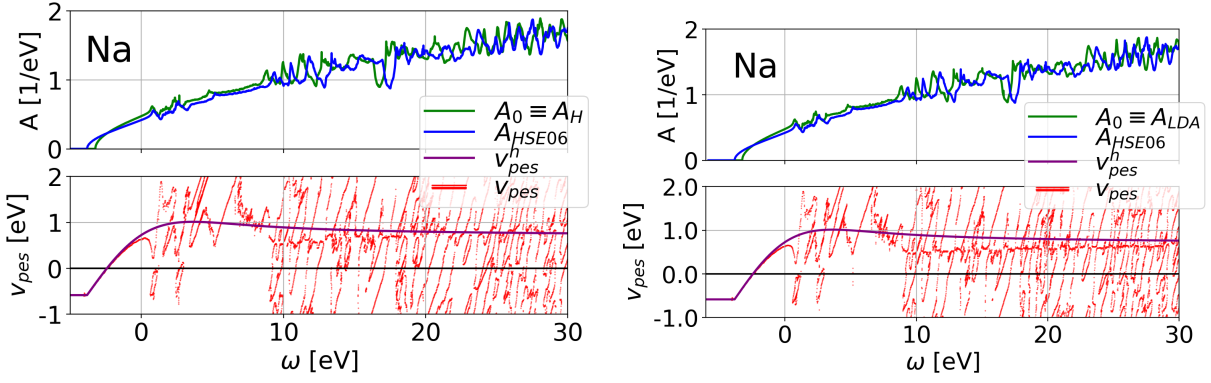


Fig. 1 Spectral functions of sodium: the target HSE06 (blue lines) is obtained from the starting spectral functions (green lines) thanks to the potential $v_{pes}(\omega)$ (red lines, in eV). The starting spectral function is calculated within the Hartree approximation (left panels) or the LDA (right panels). The approximated $v_{pes}(\omega)$ obtained from the HEG following Eq. (12) is represented by the purple lines.

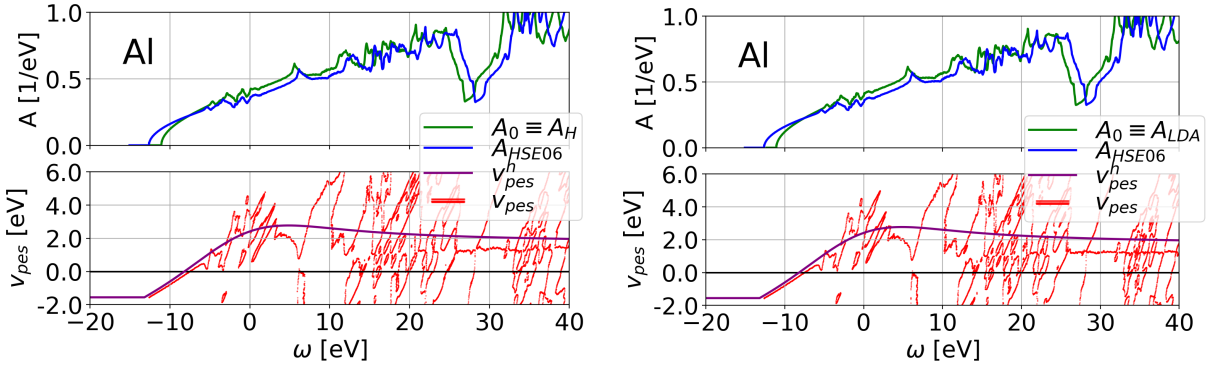


Fig. 2 Spectral functions of aluminum: the target HSE06 (blue lines) is obtained from the starting spectral functions (green lines) thanks to the potential $v_{pes}(\omega)$ (red lines, in eV). The starting spectral function is calculated within the Hartree approximation (left panels) or the LDA (right panels). The approximated $v_{pes}(\omega)$ obtained from the HEG following Eq. (12) is represented by the purple lines.

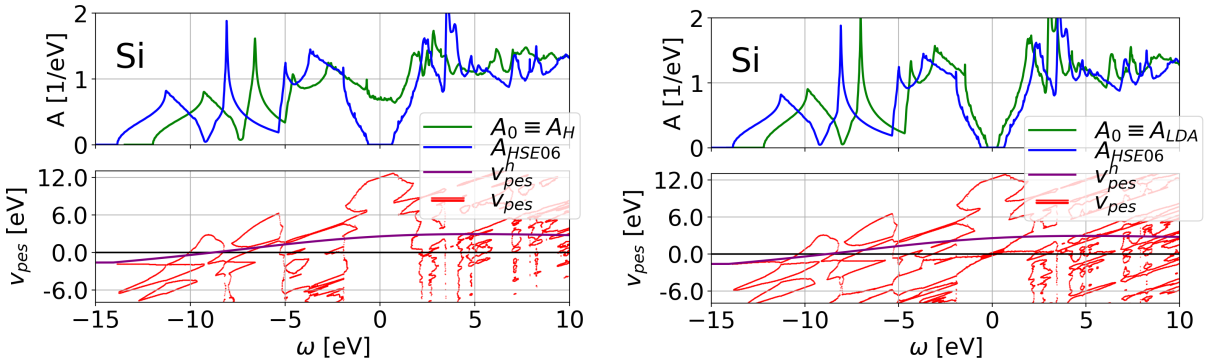


Fig. 3 Spectral functions of silicon: the target HSE06 (blue lines) is obtained from the starting spectral functions (green lines) thanks to the potential $v_{pes}(\omega)$ (red lines, in eV). The starting spectral function is calculated within the Hartree approximation (left panels) or the LDA (right panels). The approximated $v_{pes}(\omega)$ obtained from the HEG following Eq. (12) is represented by the purple lines.

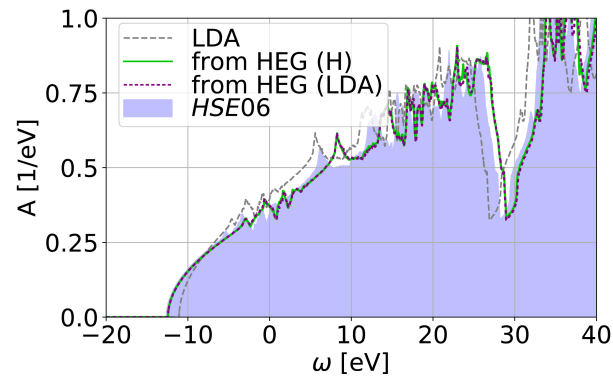
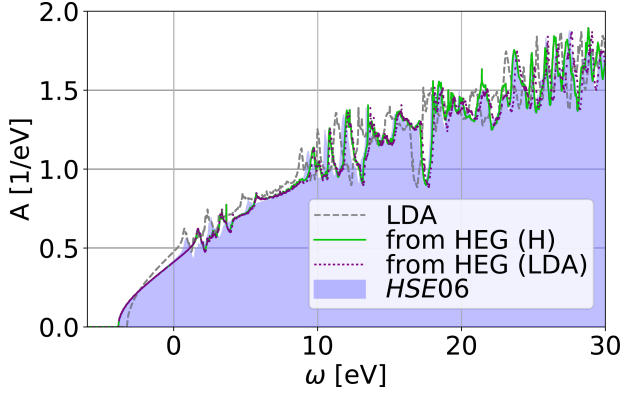


Fig. 4 Using Eq. (9) and (12) to build the spectral function of Na (upper panel) and Al (bottom panel), starting from the Hartree approximation (green) or the LDA (purple). The shaded area is the target HSE06 spectral function.

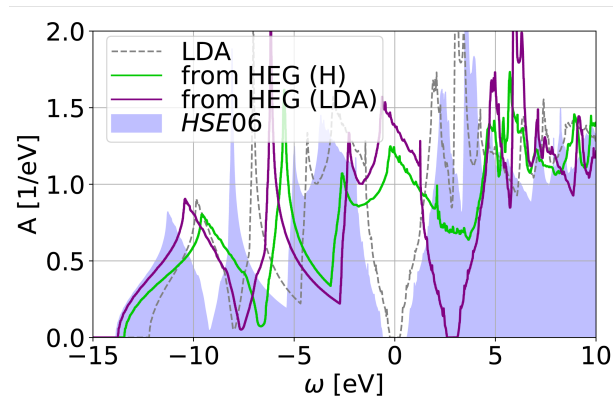


Fig. 5 Using Eq. (9) and (12) to build the spectral function of Si, starting from the Hartree approximation (green) or the LDA (purple). The shaded area is the target HSE06 spectral function.

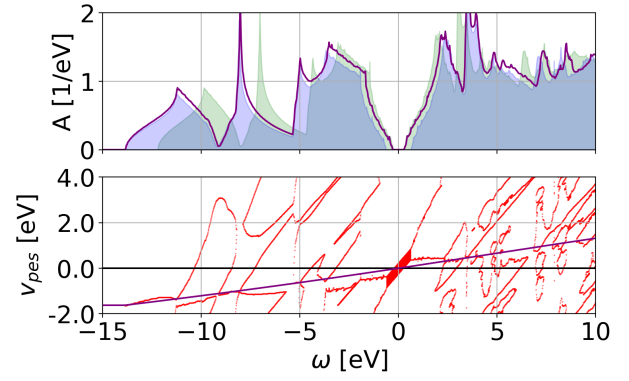


Fig. 6 Upper panel: in purple, the spectral function of Si, obtained by replacing eq. (12) with a two-parameters connector, eq. (13). The shaded purple area is the target result, while the green area is the starting point spectral function (LDA). Lower panel: the fitting of the potential via eq. (13).

the target result, considering the minimum effort required. The improvement with respect to the LDA result is clear. On the other hand, other small features (see, e.g., the bunch of peaks at ~ 3 eV in sodium, or the ones around the Fermi energy in aluminum) are not well reproduced. In fact, those features correspond to gaps that open up in correspondence of Brillouin zone boundaries²². Those features are intrinsically related to the presence of the potential of the crystal. Therefore, it is expected that a more elaborate connector, with more physical information from the material, is needed in these regions.

Also for silicon, see Fig. 5, the bottom of the valence band is quite well reproduced by this effective method. However, the difference in the choice of the starting point is noteworthy: while starting from the Hartree spectral function results in a good value for the bottom of the band, starting from LDA results in a true quantitative agreement. Also for the rest of the spectrum, the choice of LDA as a starting point offers a much better result with respect to Hartree. The latter is in fact not able to open a gap, while the former does, even though at too high energy, around 3 eV. The fact that the results in silicon are not as good as in metals is not surprising. Silicon is much farther from the HEG than sodium and aluminum, and the connector of Eq. (12), a rigid shift and a single value for the density (the average density), is too crude.

A simple improvement is, for instance, adding a scaling factor in the frequency argument of the HEG potential, and fitting the physical potential with two free parameters a and b at the bottom of the valence band and the gap region, see lower panel of fig. 6. This gives as a result:

$$v_{\text{pes}}^h(\omega) = v_{\text{pes}|n^h=\bar{n}}^h(a(\omega - \mu + \mu^h) + b). \quad (13)$$

This reminds a quasiparticle expansion of the spectral function around the Fermi energy in Fermi liquids⁵⁶. The parameter a acts as renormalization factor, while b as further corrector to the Fermi level alignment. This renormalization effectively changes the bandwidths. The fact that $a \neq 1$ implies that the renormali-

sation in the frequency-dependent potential occurs differently in the HEG and in silicon. The reason why this occurs and how the connector approximation should take it into account is a very interesting open question that is worth further investigation beyond the present work. The result, obtained with $a = 0.39$ and $b = -8.7$ eV, is shown in Fig. 6: both the valence as well as the conduction band are very well reproduced. Only in the gap region, the HEG potential is not strong enough to considerably depart from the starting point.

To summarize, simple modifications on the HEG potential are enough to yield very good results in the spectral function. From our analysis we can conclude that the simple connector (12) is already a promising starting point to devise approximations for the scalar potential $v_{\text{pes}}(\omega)$. Therefore, this new efficient auxiliary potential is a route that is worth to explore further. In particular, we can imagine to know the spectral function of a given material (from experiment or an accurate calculation) and we can think of using $v_{\text{pes}}(\omega)$ to have a very good estimation of the spectral functions of materials belonging to same class of materials. Here we have shown that knowing the potential in the HEG leads to very good spectral functions for sodium and aluminum at an almost zero computational cost. On the other hand, we also see a limit in the design of effective potentials that have such a simple mathematical form. For materials that are far from the model system, finding a good connector could become a difficult task.

4 Optical spectroscopy

4.1 State of the art: TDDFT and BSE

Absorption spectra of solids are described by the imaginary part of the macroscopic dielectric function $\epsilon_M(\omega)$, which can be calculated from¹

$$\epsilon_M(\omega) = 1 - \lim_{\mathbf{q} \rightarrow 0} v_{\mathbf{G}=0}(\mathbf{q}) \bar{\chi}_{\mathbf{G}=0, \mathbf{G}'=0}(\mathbf{q}, \omega) \quad (14)$$

where \mathbf{G} and \mathbf{G}' are reciprocal-lattice vectors. In the long-wavelength limit $\mathbf{q} \rightarrow 0$, absorption spectra are hence given by the imaginary part of the product between the long-range term ($\mathbf{G} = 0$) of the Coulomb interaction v and the head ($\mathbf{G} = \mathbf{G}' = 0$) matrix element of the density response $\bar{\chi}$ to the total macroscopic classical potential.

Within TDDFT $\bar{\chi}$ can be obtained as a solution of the Dyson-like equation^{1,57}:

$$\bar{\chi}(12) = \chi_0(12) + \chi_0(13)[\bar{v}(34) + f_{\text{xc}}(34)]\bar{\chi}(42) \quad (15)$$

where χ_0 is the Kohn-Sham density-response function, \bar{v} is the Coulomb interaction without its long-wavelength component, and f_{xc} is the xc kernel. In Eq. (15) repeated indexes are integrated over and we have adopted the short-hand notation (1) for the space-time indexes (\mathbf{r}_1, t_1) .

In Eq. (15) the f_{xc} kernel needs to be approximated. Setting $f_{\text{xc}} = 0$ corresponds to the random-phase approximation⁵⁸ (RPA): $\bar{\chi} = \bar{\chi}^{\text{RPA}}$, which completely misses excitonic effects. The most widely used adiabatic local density approximation (ALDA) to f_{xc} improves over the RPA in the description of plasmon excitations in loss spectra, but still fails to capture excitonic ef-

fects in the optical spectra of extended systems⁵⁹. In line with literature, here we also introduce a many-body xc kernel $f_{\text{xc}}^{\text{mb}}$, formally defined by replacing $\chi_0(12)$ by the independent-particle $P_0(12) = -iG(12)G(21)$ in (15), where G are interacting Green's functions. In practice, P_0 is usually built from a quasiparticle band structure in the GWA, which makes the task of the remaining part of the kernel easier, since one starts from the correct band gap.

Within MBPT $\bar{\chi}$ instead is obtained from the diagonal

$$\bar{L}(1122) = \bar{\chi}(12), \quad (16)$$

where the (modified) two-particle correlation function $\bar{L}(1234)$ is the solution of the Bethe-Salpeter equation^{60,61} (BSE):

$$\bar{L}(1234) = L_0(1234) + L_0(1256)[\bar{v}(57)\delta(56)\delta(78) + \Xi(5678)]\bar{L}(7834) \quad (17)$$

in the charge sector. Here $L_0(1234) = -iG(13)G(42)$ is the independent-particle correlation function whose diagonal is $L_0(1122) = P_0(12)$, and Ξ is the electron-hole interaction kernel. In the most widely used approximation⁶²⁻⁶⁵, the GWA is adopted to calculate G and the derivative that yields Ξ . Moreover, the quasi-particle approximation is used for G , and Ξ is approximated by the statically screened Coulomb interaction $\Xi(5678) = -W^{st}(56)\delta(57)\delta(68)$.

The solution of the BSE in the GWA represents the state-of-the-art approach for the successful calculation of optical spectra and exciton properties in a large variety of materials^{1,5}. In the strongly correlated regime DMFT analysis of the BSE within the Hubbard model shows divergence of BSE at the Mott transition^{66,67}. Singularities of the irreducible vertexes which enter as a kernel in BSE⁶⁸ are found within the same formalism. However these divergences, which occur inside the Fermi-liquid phase, though not necessarily related to the proximity of a Mott transition, are certainly associated to a non-perturbative behaviour of strongly interacting system⁶⁹, which is beyond the scope of the present paper. In the following we will consider only *sp* semiconductors and insulators, where the GWA-BSE is in very good agreement with experiments^{1,5}.

The goal of much work over the last two decades has been directed to combine the best of the two frameworks¹, namely to reduce the computational cost of the BSE thanks to the use of TDDFT, while keeping the same level of accuracy. By defining a four-point TDDFT response function ${}^4\bar{\chi}$ such that

$${}^4\bar{\chi}(1122) = \bar{\chi}(12), \quad (18)$$

it is possible to formally combine the TDDFT and BSE Dyson-like equations (15) and (17) to give

$$\bar{L}(1234) = {}^4\bar{\chi}(1234) + {}^4\bar{\chi}(1256) \left[\Xi(5678) - f_{\text{xc}}^{\text{mb}}(57)\delta(56)\delta(78) \right] \bar{L}(7834). \quad (19)$$

By imposing the conditions (16) and (18) in Eq. (19), we obtain a generalized Sham-Schlüter equation^{19,38} for $f_{\text{xc}}^{\text{mb}}$:

$$f_{\text{xc}}^{\text{mb}}(34) = \bar{\chi}^{-1}(31){}^4\bar{\chi}(1156)\Xi(5678)\bar{L}(7822)\bar{\chi}^{-1}(24) \quad (20)$$

which establishes an exact connection between TDDFT and MBPT quantities.

The Nanoquanta f_{xc}^{mb} kernel^{19,41–46} of TDDFT is obtained from a first-order linearization of Eq. (20), with $\tilde{\chi} \rightarrow P_0 = -iGG$ and $\bar{L} \rightarrow P_0$, and the usual GWA to the BSE kernel $\Xi = -W^{st}$:

$$f_{xc}^{mb}(12) = P_0^{-1}(13)G(34)G(53)W^{st}(45)G(46)G(65)P_0^{-1}(62). \quad (21)$$

This kernel (21) gives results close to BSE ones. However, although it is used within the formalism of TDDFT, calculations are still cumbersome. In the next subsection we will investigate the possibility to design effective kernels for optical absorption that are simpler than the f_{xc} or f_{xc}^{mb} of TDDFT.

It is interesting to investigate the relation between the Nanoquanta approximation and the non-locality of the self-energy. Schematically, the contribution $\bar{L}\tilde{\chi}^{-1}$ in (20) is $(\delta G/\delta v_{cl,m})(\delta v_{cl,m}/\delta n)$ with $v_{cl,m}$ the sum of external and macroscopic Hartree potential. Changing the chain rule, this is equal to $(\delta G/\delta v_{eff})(\delta v_{eff}/\delta n)$, where v_{eff} can be any local potential that is in one-to-one relation with the density, such as, e.g., the Hartree potential, or the Kohn-Sham potential. If G was the result of a total local potential v_{tot} , then one could use $v_{eff} = v_{tot}$ in the chain rule, and (21) would be exact. However, G cannot be obtained from any local potential. Indeed, the more the self-energy is non-local, the more the Nanoquanta approximation will degrade the spectra. This also has practical consequences: the non-locality of the GW self-energy is encoded in the non-locality of W . In reciprocal space, this is reflected in the contributions $W(\mathbf{q})$ for small wavevector \mathbf{q} . In practice one uses a discrete sampling of the Brillouin zone, and the most problematic, long-range contribution is the one due to the region around $\mathbf{q} \rightarrow 0$. Since this is just a constant, it can be included in P_0 from the beginning, as explained in Ref.⁴⁴, and is therefore not approximated. This is also the strategy used in the present work. However, for an increasingly dense sampling of the Brillouin zone more and more contributions with small \mathbf{q} arise that cannot be avoided in this simple way. This limits the degree to which a spectrum based on the Nanoquanta kernel can be converged.

4.2 Effective kernels for absorption

While TDDFT is aimed at giving the whole two-point polarizability $\tilde{\chi}(12)$ and the BSE the whole four-point correlation function $\bar{L}(1234)$, optical absorption only measures an integral over a diagonal, namely the imaginary part of the frequency-dependent function $\mathbb{A}_{\mathbf{q}}(\omega)$, defined for each wavevector \mathbf{q} as:

$$\begin{aligned} \mathbb{A}_{\mathbf{q}}(\omega) &= \tilde{\chi}_{G=0, G'=0}(\mathbf{q}, \omega) = \int d\mathbf{r}_1 d\mathbf{r}_2 \tilde{\chi}(\mathbf{r}_1, \mathbf{r}_2, \omega) e^{i\mathbf{q}(\mathbf{r}_1 - \mathbf{r}_2)} \\ &= \int d12 \bar{L}(1122) e^{i\mathbf{q}(\mathbf{r}_1 - \mathbf{r}_2)} e^{i\omega(t_1 - t_2)}. \end{aligned} \quad (22)$$

We can hence identify $\mathbb{A}_{\mathbf{q}}(\omega)$ as our target for which we can introduce other effective kernels for new auxiliary systems that are simpler than TDDFT and the BSE. The design of a new auxiliary system always implies finding a compromise between the simplicity of the *ansatz* for the effective kernel and the difficulty one has

then to face for its approximation. To illustrate this general issue, in the following we will compare three different possibilities for effective kernels designed to yield $\mathbb{A}_{\mathbf{q}}(\omega)$, in principle exactly.

The simplest choice, for each wavevector \mathbf{q} , is a scalar kernel^{70,71}:

$$f_{\mathbf{q}}^{abs}(\omega) = \frac{1}{\mathbb{A}_{\mathbf{q}}^{RPA}(\omega)} - \frac{1}{\mathbb{A}_{\mathbf{q}}(\omega)} \quad (23)$$

or

$$f_{\mathbf{q}}^{abs,mb}(\omega) = \frac{1}{\mathbb{A}_{\mathbf{q}}^{RPA,mb}(\omega)} - \frac{1}{\mathbb{A}_{\mathbf{q}}(\omega)} \quad (24)$$

depending whether the RPA quantities $\mathbb{A}_{\mathbf{q}}^{RPA}(\omega) = \tilde{\chi}_{G=0, G'=0}^{RPA}(\mathbf{q}, \omega)$ or $\mathbb{A}_{\mathbf{q}}^{RPA,mb}(\omega) = \tilde{\chi}_{G=0, G'=0}^{RPA,mb}(\mathbf{q}, \omega)$ include Kohn-Sham or MBPT ingredients. These new effective scalar kernels for absorption spectroscopy have a much simpler form than the corresponding TDDFT kernels (see Sec. 4.1):

$$(f_{xc})_{G, G'}(\mathbf{q}, \omega) = (\tilde{\chi}^{RPA})_{G, G'}^{-1}(\mathbf{q}, \omega) - (\tilde{\chi})_{G, G'}^{-1}(\mathbf{q}, \omega) \quad (25)$$

$$(f_{xc}^{mb})_{G, G'}(\mathbf{q}, \omega) = (\tilde{\chi}^{RPA,mb})_{G, G'}^{-1}(\mathbf{q}, \omega) - (\tilde{\chi})_{G, G'}^{-1}(\mathbf{q}, \omega) \quad (26)$$

which are instead matrices in reciprocal space. On the other hand, being a more compact object, the frequency dependence of a scalar kernel may be wilder than for the full TDDFT kernel, since f^{abs} has to fold the spatial non-locality of f_{xc} into its frequency dependence¹⁹. In particular, f^{abs} is generally different from the head element of f_{xc} (see also Ref.⁷⁰).

At the place of the TDDFT Dyson equation (15), one has:

$$\mathbb{A}_{\mathbf{q}}(\omega) = \mathbb{A}_{\mathbf{q}}^0(\omega) + \mathbb{A}_{\mathbf{q}}^H(\omega) + \mathbb{A}_{\mathbf{q}}^0(\omega) f_{\mathbf{q}}^{abs,mb}(\omega) \mathbb{A}_{\mathbf{q}}(\omega) \quad (27)$$

where $\mathbb{A}_{\mathbf{q}}^0(\omega)$ is the head matrixelement of P_0 :

$$\mathbb{A}_{\mathbf{q}}^0(\omega) = P_{G=0, G'=0}^0(\mathbf{q}, \omega). \quad (28)$$

and

$$\mathbb{A}_{\mathbf{q}}^H(\omega) = \sum_{G_1} P_{G=0, G_1}^0(\mathbf{q}, \omega) \bar{v}_{G_1}(\mathbf{q}) \tilde{\chi}_{G_1, G'=0}(\mathbf{q}, \omega). \quad (29)$$

We can now make a direct comparison with the head ($G = G' = 0$) matrix elements derived from the BSE (17):

$$\mathbb{A}_{\mathbf{q}}(\omega) = \mathbb{A}_{\mathbf{q}}^0(\omega) + \mathbb{A}_{\mathbf{q}}^H(\omega) + \mathbb{A}_{\mathbf{q}}^{BSE,xc}(\omega) \quad (30)$$

where we have used the fact that P_0 and $\tilde{\chi}$ are the diagonal of L_0 and \bar{L} , respectively (see Sec. 4.1), and we have defined:

$$\mathbb{A}_{\mathbf{q}}^{BSE,xc}(\omega) = \int d123456 L_0(1134) \Xi(3456) \bar{L}(5622) e^{i\mathbf{q}(\mathbf{r}_1 - \mathbf{r}_2)} e^{i\omega(t_1 - t_2)} \quad (31)$$

(where the space-time integrals have been made explicit for clarity). In this way we can easily relate the two frameworks (see Eqs. (27) and (30)) and find:

$$f_{\mathbf{q}}^{abs,mb}(\omega) = \frac{\mathbb{A}_{\mathbf{q}}^{BSE,xc}(\omega)}{\mathbb{A}_{\mathbf{q}}^0(\omega) \mathbb{A}_{\mathbf{q}}(\omega)}. \quad (32)$$

Eq. (32) is very appealing: for each frequency, it is just a ratio of two complex numbers. So far no approximation has been made: by construction this kernel gives the same spectra as those obtained from the BSE. However, since it is defined in terms of the same quantities that one aims to calculate, Eq. (32) is of no direct

practical use. Still it remains very useful as a starting point to derive valuable approximations. Here we follow the same strategy outlined in Sec. 4.1 for the Nanoquanta kernel (21) of TDDFT. We adopt the first-order approximations: $\bar{L} = P_0 = -iGG$, and take the static GWA for the BSE kernel $\Xi = -W^{st}$. This for $\mathbb{A}_{\mathbf{q}}^{\text{BSE,xc}}(\omega)$, i.e. the numerator of Eq. (32), leads to:

$$\mathbb{A}_{\mathbf{q}}^{\text{GWA-BSE}}(\omega) = \int d1234 G(13)G(41)W^{st}(34)G(32)G(24) \times e^{i\mathbf{q}(\mathbf{r}_1-\mathbf{r}_2)} e^{i\omega(t_1-t_2)}. \quad (33)$$

In order to benefit from error cancelling, we make the corresponding approximation to the quantities appearing at the denominator of Eq. (32). The result is the approximated expression:

$$f_{\mathbf{q}}^{\text{abs,mb},0}(\omega) = \frac{\mathbb{A}_{\mathbf{q}}^{\text{GWA-BSE}}(\omega)}{[\mathbb{A}_{\mathbf{q}}^0(\omega)]^2}. \quad (34)$$

In a system with a non-zero band gap (i.e., a semiconductor or an insulator), in the optical limit $\mathbf{q} \rightarrow 0$ both $\mathbb{A}_{\mathbf{q}}^{\text{GWA-BSE}}$ and $\mathbb{A}_{\mathbf{q}}^0(\omega)$ go to zero^{41,72,73} as q^2 . As a result, in this limit the scalar kernel (34) is proportional to $f(\omega)/q^2$. In Ref.⁷⁴ the particular form of the function $f(\omega) = -\alpha + \beta\omega^2$ was proposed for the dynamical long-range contribution of the TDDFT f_{xc} kernel, where the parameters α and β were empirically related to the dielectric constant and the plasma frequency. It was shown that the absorption spectra of large gap insulators are improved with respect to calculations where the kernel is taken to be static⁷⁵. We can also compare the kernel (34) with the scalar version of the bootstrap TDDFT kernel^{76,77} $f_{xc}^{\text{BO}} = 1/[\epsilon_M(\omega = 0)\delta_{\mathbf{q}}^0(\omega = 0)]$. Both share the same q dependence, but the bootstrap TDDFT kernel is static (and hence also real). This property of bootstrap kernels has been identified as the reason why it leads to spectra with excitonic features with too large intensities[¶] in the spectra^{77,78}.

The scalar kernel $f_{\mathbf{q}}^{\text{abs}}(\omega)$ (23) is not the only possible choice. In the 1970s, a contact exciton model was put forward for optical spectra of semiconductors that was based on a contact electron-hole interaction^{71,79-81}: $C\delta(\mathbf{r}-\mathbf{r}')$. Here we can make this model exact if we introduce an *ansatz* for another auxiliary system with a kernel that is diagonal in reciprocal space^{||}: $f_{\mathbf{q}}^{\text{conex}}(\omega)\delta_{\mathbf{G}_1,\mathbf{G}_2}$; each matrix element in the reciprocal space is the same complex frequency-dependent function. To this end we formulate a new Dyson equation:

$$X_{\mathbf{G},\mathbf{G}'}(\mathbf{q},\omega) = P_{\mathbf{G},\mathbf{G}'}^0(\mathbf{q},\omega) + \sum_{\mathbf{G}_1,\mathbf{G}_2} P_{\mathbf{G},\mathbf{G}_1}^0(\mathbf{q},\omega) [\bar{v}_{\mathbf{G}_1}(\mathbf{q}) + f_{\mathbf{q}}^{\text{conex}}(\omega)] \delta_{\mathbf{G}_1,\mathbf{G}_2} X_{\mathbf{G}_2,\mathbf{G}'}(\mathbf{q},\omega). \quad (35)$$

In this new relation the effective susceptibility X is designed in such a way that, for each \mathbf{q} , its head matrixelement is:

$X_{\mathbf{G}=0,\mathbf{G}'=0}(\mathbf{q},\omega) = \mathbb{A}_{\mathbf{q}}(\omega) = \bar{\chi}_{\mathbf{G}=0,\mathbf{G}'=0}(\mathbf{q},\omega)$. All other elements $\mathbf{G},\mathbf{G}' \neq 0$, in principle, may instead differ from the TDDFT response function $\bar{\chi}$.

By making use of these properties, the contact exciton kernel $f_{\mathbf{q}}^{\text{conex}}$ can be related to the BSE, analogously to what has been done for the scalar kernel $f^{\text{abs,mb},0}$ in Eq. (32). The result is:

$$f_{\mathbf{q}}^{\text{conex}}(\omega) = \frac{\mathbb{A}_{\mathbf{q}}^{\text{BSE,xc}}(\omega)}{\sum_{\mathbf{G}_1} P_{\mathbf{G}=0,\mathbf{G}_1}^0(\mathbf{q},\omega) X_{\mathbf{G}_1,\mathbf{G}'=0}(\mathbf{q},\omega)}. \quad (36)$$

Compared to Eq. (32), the numerator remains the same, while the denominator is now built with the new effective function entering the Dyson equation (35). We can therefore make similar first-order approximations as in Eq. (34) and obtain:

$$f_{\mathbf{q}}^{\text{conex}}(\omega) = \frac{\mathbb{A}_{\mathbf{q}}^{\text{GWA-BSE}}(\omega)}{\sum_{\mathbf{G}_1} P_{\mathbf{G}=0,\mathbf{G}_1}^0(\mathbf{q},\omega) P_{\mathbf{G}_1,\mathbf{G}=0}^0(\mathbf{q},\omega)}. \quad (37)$$

The product of two head matrixelements of P_0 at the denominator of Eq. (34) is now replaced by a scalar product of two wings of P_0 , i.e. the elements of the matrix in the reciprocal space for which either \mathbf{G} or \mathbf{G}' are zero. The wing matrixelements of P_0 in an insulator for $\mathbf{q} \rightarrow 0$ go to 0 as q . In contrast to the scalar kernel (34), this contact exciton kernel (37) in the optical limit is hence not divergent. If instead of the Dyson equation (35) one solved a scalar equation for the head elements $\mathbf{G} = \mathbf{G}' = 0$ only, the contact exciton kernel (37) in an insulator would not change the RPA spectrum obtained from $\bar{\chi}^{\text{RPA,mb}}$. The contact exciton kernel (37) can produce a visible effect on the calculated spectrum because it is employed for all the diagonal elements $\mathbf{G}_1 = \mathbf{G}_2$ in the double sum in the second line of Eq. (35). Indeed, a static version of (36) was already examined in Ref.⁸¹. The conclusion was that a static contact exciton kernel is able to create a bound exciton in the band gap, but at the same time is incapable to produce more than one bound exciton or describe excitons in the continuum of electron-hole transitions above the band gap. The dynamical contact exciton (36), and its approximated version (37), can in principle overcome these limitations.

One could also explicitly impose to the new effective kernel some known properties of other more complex kernels. In particular, it is well known^{41,73} that the TDDFT f_{xc}^{mb} kernel in insulators needs to have a long-range contribution in real space as the Coulomb interaction. So one could exploit this specific dependence on the momentum transfer \mathbf{q} of f_{xc}^{mb} to design a better *ansatz* in the Dyson equation (35). The question would be whether a linear approximation would be less severe leading to better results. To this end, we replace the contact exciton kernel in the Dyson equation (35) with a kernel that explicitly displays a long-range component:

$$\bar{X}_{\mathbf{G},\mathbf{G}'}(\mathbf{q},\omega) = P_{\mathbf{G},\mathbf{G}'}^0(\mathbf{q},\omega) + \sum_{\mathbf{G}_1,\mathbf{G}_2} P_{\mathbf{G},\mathbf{G}_1}^0(\mathbf{q},\omega) \left[\bar{v}_{\mathbf{G}_1}(\mathbf{q}) + \frac{f_{\mathbf{q}}^{\text{LR}}(\omega)}{|\mathbf{q} + \mathbf{G}_1|^2} \right] \delta_{\mathbf{G}_1,\mathbf{G}_2} \bar{X}_{\mathbf{G}_2,\mathbf{G}'}(\mathbf{q},\omega). \quad (38)$$

¶ The bootstrap kernel gives also too small binding energies for bound excitons, which can be improved with refined variants^{77,78}.

|| The real and static ALDA kernel of TDDFT has the form: $f_{xc}(\mathbf{r},\mathbf{r}') = f(\mathbf{r})\delta(\mathbf{r}-\mathbf{r}')$, which becomes a matrix in reciprocal space: $f_{\mathbf{G},\mathbf{G}'}^{\text{xc}} = f(\mathbf{G}-\mathbf{G}')$.

Here the kernel has the same long-range term as the f_{xc}^{mb} kernel, but is still designed to yield only the head of $\tilde{\chi}$ and not the whole matrix. Introducing a first-order approximation along the same lines as Eq. (37), we finally get to:

$$f_{\mathbf{q}}^{LR}(\omega) = \frac{\mathbb{A}_{\mathbf{q}}^{GWA-BSE}(\omega)}{\sum_{\mathbf{G}_1} \frac{P_{\mathbf{G}=0,\mathbf{G}_1}^0(\mathbf{q},\omega)P_{\mathbf{G}_1,\mathbf{G}=0}^0(\mathbf{q},\omega)}{|\mathbf{q} + \mathbf{G}_1|^2}}. \quad (39)$$

In the next section we will compare the three kernels (34)-(37)-(39) and we will benchmark the three approximations for the optical absorption spectra of silicon, LiF and solid argon.

4.3 Absorption spectra

Fig. 7 shows the scalar kernels $f^{abs}(\omega)$ and $f^{abs,mb}(\omega)$ for $\mathbf{q} \rightarrow 0$ obtained by reverse engineering. To this end, we directly use the definitions (23) and (24), where $\mathbb{A}_{\mathbf{q}}(\omega)$ is calculated within the GWA-BSE that gives accurate absorption spectra in silicon, LiF and solid argon (see black lines in Fig. 8). The difference between the two effective kernels is that while $f^{abs,mb}(\omega)$ has only to describe attractive electron-hole (i.e. excitonic) effects, $f^{abs}(\omega)$ also has to account for the band-gap opening from the LDA to the GWA. As also previously found^{70,71}, both kernels are strongly frequency dependent. In the low-energy region (before strong oscillations start to develop in correspondence to poles of the response functions), the signs of the two kernels $f^{abs}(\omega)$ and $f^{abs,mb}(\omega)$ are opposite: they effectively shift the weight of the absorption spectra to larger or smaller energies, respectively. The imaginary part of $f^{abs,mb}(\omega)$ is zero until the onset of the spectrum (see Fig. 8), while the imaginary part of $f^{abs}(\omega)$ is as important as its corresponding real part already beyond the LDA direct band gap (see vertical dotted lines in Fig. 7): its contribution is needed in order to achieve the band-gap opening^{82,83}.

We can now examine in detail the two aspects: (i) what is the effect of their imaginary parts? (ii) how important is their frequency dependence?

To answer the first of these questions, we calculate the absorption spectra of the three materials by using only the real parts of the kernel and compare the results with the GWA-BSE spectra that would be instead obtained with the full kernels. The results, shown in Fig. 8, are completely different for the two effective kernels. The absence of the imaginary part of $f^{abs}(\omega)$ kernel completely destroys the spectrum (see orange lines), thus indicating its key contribution. On the contrary, the real-only many-body version of the kernel $f^{abs,mb}(\omega)$ is still capable to produce spectra with excitonic features at the correct positions (see green lines). Its imaginary part now has only a minor role: it mainly gives rise to the damping of the peaks, which are too intense and narrow if one neglects its contribution.

To answer the second question, we recalculate the spectra by using two static kernels obtained by evaluating $f^{abs,mb}(\omega)$, respectively, at $\omega = 0$ or at $\omega = E_{\lambda}$, where E_{λ} are the energies of the prominent exciton peaks in Si ($E_{\lambda} = 3.2$ eV), LiF ($E_{\lambda} = 13.1$ eV) and Ar ($E_{\lambda} = 12.3$ eV). The static kernel $f^{abs,mb}(\omega = 0)$ has only a non-zero real part: in all cases, it is incapable to produce a sensible spectrum (see blue lines in Fig. 8). The other static ker-

nel $f^{abs,mb}(\omega = E_{\lambda})$ instead gives rise to a single bound exciton peak (see magenta lines in Fig. 8). Its binding energy is slightly overestimated with respect to the BSE in LiF and Ar, while its width is exaggerated as a consequence of the large imaginary part of $f^{abs,mb}(\omega = E_{\lambda})$. By suppressing it, the peak position doesn't change but the peak becomes too narrow (not shown), confirming the previous analysis. We can therefore conclude that the frequency dependence of the effective kernels plays a key role in order to obtain spectra of the same quality of the BSE. The ability to reproduce this frequency dependence will determine the quality of the approximations.

We can now assess the validity of the Nanoquanta-like approximations to the various effective kernels introduced in Sec. 4.2: (i) the scalar kernel $f_{\mathbf{q}}^{abs,mb,0}(\omega)$, see Eq. (34) (red line in Figs. 9-10); (ii) the contact exciton kernel $f_{\mathbf{q}}^{conex}(\omega)$, see Eq. (37) (blue line in Figs. 9-10); (iii) the long-range kernel $f_{\mathbf{q}}^{LR}(\omega)$, see Eq. (39) (orange line in Figs. 9-10).

Fig. 9 compares the real and imaginary parts of these three approximations with the same reference effective many-body kernel $f^{abs,mb}(\omega)$ that we have analysed in Fig. 7. In both their real and imaginary parts, they all qualitatively follow the reference kernel, with oscillations of the same sign that begin after the onset of the spectra. However, in all the cases, quantitative discrepancies among the different kernels are apparent in both the locations and the amplitudes of these oscillations. In order to appreciate the importance of these differences, we have to examine the spectra that they produce.

Fig. 10 compares the BSE reference spectrum (black line) with the absorption spectra obtained within the Nanoquanta approximations to different kernels. The only reliable result is obtained from the Nanoquanta approximation to the TDDFT xc kernel $f_{xc}^{mb}(\mathbf{r},\mathbf{r}',\omega)$, see Eq. (21) (see magenta line). All the other spectra, obtained by applying analogous approximations to the other effective kernels, are not accurate enough. They are all capable to reproduce excitonic effects to a certain extent, resulting in spectra shifted to lower energies with respect to the GW-RPA starting point. However, they are all in qualitative disagreement with the BSE, with results that are best in silicon and worst in argon, where the spectra even become negative.

This comparison illustrates how much the frequency dependence of the effective kernels turns out to be sensitive, and at the same time essential, to provide good results. Already at the TDDFT level, it can be understood¹⁹ as the result of an approximate folding of the spatially non-local but static BSE kernel into the frequency dependence of f_{xc}^{mb} . Operating similar linear approximations onto more compact objects, like the kernels introduced in Sec. 4.2, produces poorer results. Other more involved approximations would be needed to make them reliable as well.

5 Conclusions

In summary, we have investigated different choices of effective kernels and potentials in auxiliary systems that are designed to target specific excitation spectra, in principle exactly, while they do not necessarily yield other observables correctly. We have considered two important spectroscopies: angle-integrated photoemission and optical absorption. We have introduced new effective

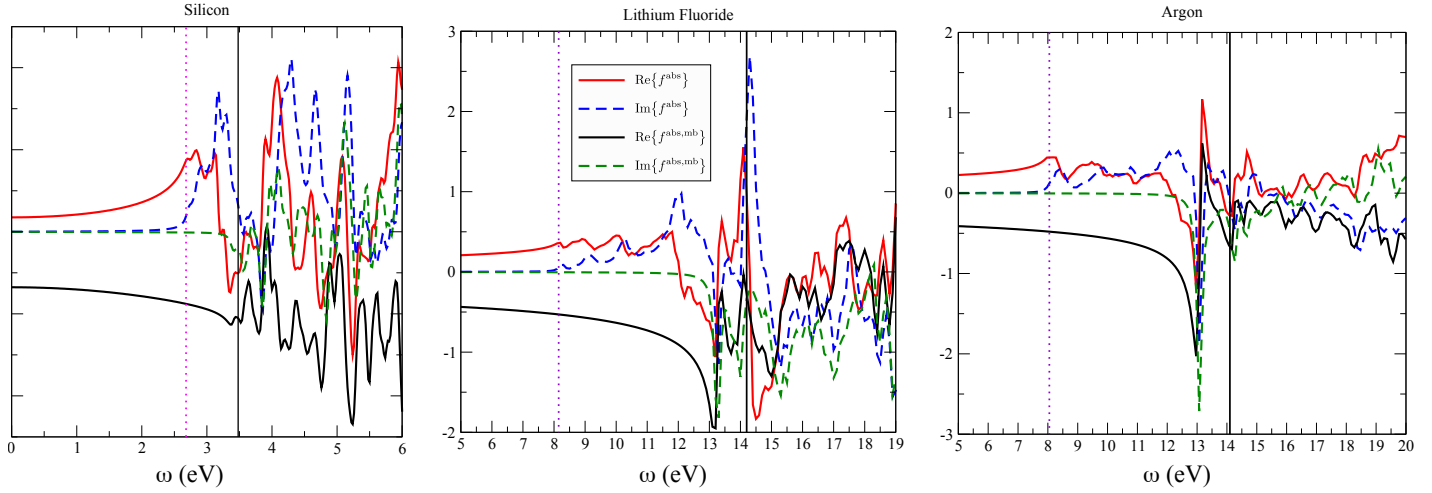


Fig. 7 Real and imaginary parts of the effective kernels for the absorption spectra of silicon (left), LiF (center) and Ar (right) (multiplied by q^2 , for a $q \rightarrow 0$ in the optical limit). These reference kernels $f^{\text{abs}}(\omega)$ and $f^{\text{abs,mb}}(\omega)$ are obtained from Eqs. (23) and (24), respectively, where $A_{\mathbf{q}}(\omega)$ gives the BSE absorption spectra (solid black line) and $A_{\mathbf{q}}^{\text{RPA,mb}}(\omega)$ the GWA-RPA spectra (dashed red line) in Fig. 8. The Kohn-Sham LDA and the GW direct band gaps are marked by the dotted violet and solid black vertical lines, respectively. $A_{\mathbf{q}}^{\text{RPA}}(\omega)$ in Eq. (23) are obtained by redshifting $A_{\mathbf{q}}^{\text{RPA,mb}}(\omega)$ by the energy distance between the two gaps (i.e., by subtracting the scissor-operator correction, see App. A).

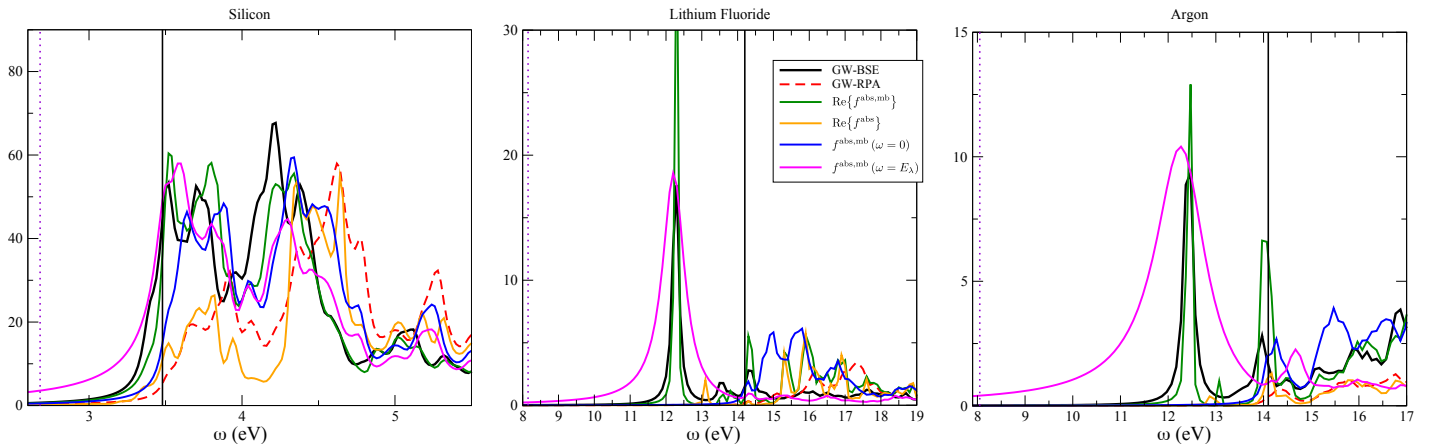


Fig. 8 The absorption spectra for silicon (left), LiF (center) and Ar (right), calculated within the GWA-RPA (which completely neglects excitonic effects, dashed red line) and the GWA-BSE (which is the reference result, solid black line) are compared with the spectra obtained: (i) using only the real parts of $f^{\text{abs,mb}}(\omega)$ and $f^{\text{abs}}(\omega)$ (green and orange lines, respectively); (ii) with only the static value $f^{\text{abs,mb}}(\omega = 0)$ (blue line); and (iii) its value at the excitonic energy $f^{\text{abs,mb}}(\omega = E_{\lambda})$ (magenta line). The excitonic value E_{λ} corresponds to 3.2 eV, 12.3 eV and 12.45 eV, for Silicon, LiF, and Ar, respectively. The spectra calculated with the full kernels $f^{\text{abs}}(\omega)$ and $f^{\text{abs,mb}}(\omega)$ (see Fig. 7) by definition would be equal to the GWA-BSE results (and hence are not shown).

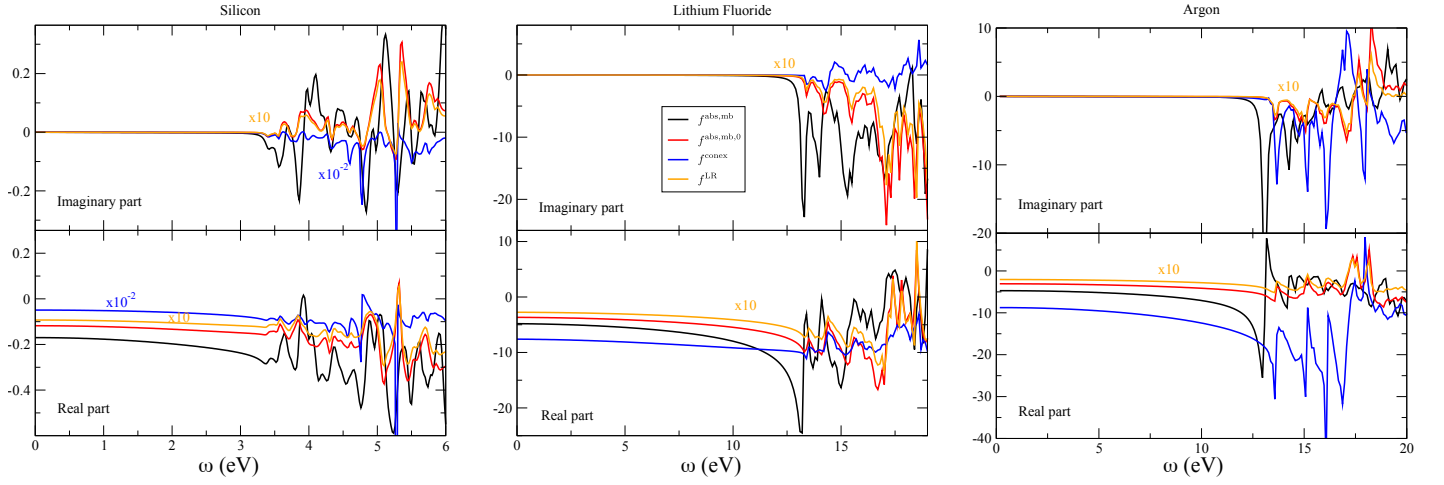


Fig. 9 Real parts (bottom panels) and imaginary parts (top panels) of the effective kernels for the absorption spectra of silicon (left), LiF (center) and Ar (right). The reference kernels $f_{\mathbf{q}}^{\text{abs,mb}}(\omega)$ (black lines, same as black and green lines in Fig. 7) are compared with the approximate kernels: (i) the scalar kernel $f_{\mathbf{q}}^{\text{abs,mb},0}(\omega)$, see Eq. (34) (red lines); (ii) the contact exciton kernel $f_{\mathbf{q}}^{\text{conex}}(\omega)$, see Eq. (37) (blue lines); (iii) the long-range kernel $f_{\mathbf{q}}^{\text{LR}}(\omega)$, see Eq. (39) (orange lines). All the kernels, except the latter two cases, are multiplied by q^2 .

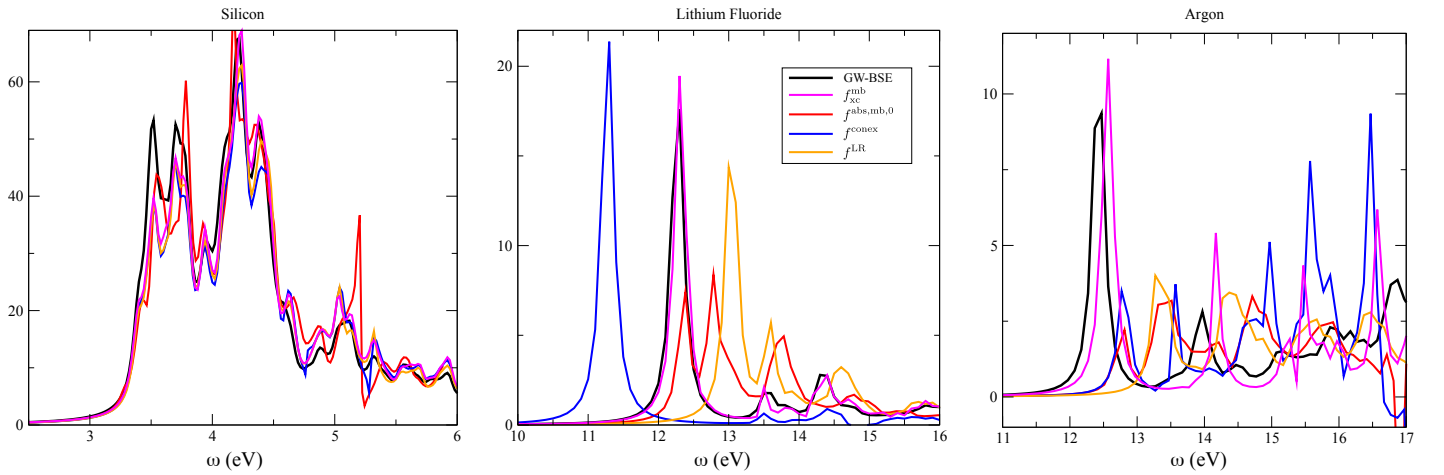


Fig. 10 The absorption spectra for silicon (left), LiF (center) and Ar (right), calculated within the GWA-BSE (which is the reference result, black line) are compared with the spectra obtained using the Nanoquanta approximations to: (i) the TDDFT xc kernel $f_{\text{xc}}^{\text{mb}}(\mathbf{r}, \mathbf{r}', \omega)$, magenta line, Eq. (21); (ii) the scalar kernel $f_{\mathbf{q}}^{\text{abs,mb},0}(\omega)$, see Eq. (34) (red line); (iii) the contact exciton kernel $f_{\mathbf{q}}^{\text{conex}}(\omega)$, see Eq. (37) (blue line); (iv) the long-range kernel $f_{\mathbf{q}}^{\text{LR}}(\omega)$, see Eq. (39) (orange line).

quantities and we have examined whether they remain amenable to approximations on the basis of physical properties of materials. To this end, we have followed two exemplary strategies of approximation for the two spectroscopies: for photoemission, we have imported the effective potential from the HEG into real materials, following the LDA philosophy of DFT and its formal generalization to the concept of connector theory; for optical absorption, inspired by the successful Nanoquanta approximation to the TDDFT kernel, we have derived approximations to the effective kernels that can be obtained, within the framework of generalized Sham-Schlüter equations, from quantities that can be accurately calculated from the BSE of MBPT. The analysis of the different choices with results for prototypical solids has allowed us to identify which are the most important properties that the kernel/potential should have built in from the beginning and which are the features that can be most easily approximated. Notably, the frequency dependence of both the scalar photoemission potential and the effective absorption kernels turns out to be their most important feature. Therefore, its accurate modeling will be the most delicate aspect for their use.

This investigation leads us to argue that there is much room for working directly with reduced quantities and the corresponding auxiliary systems targeting specific excitation spectra for spectroscopy. Having at disposal a palette of effective potentials and kernels with different degrees of complexity opens up the possibility to choose, in each situation, the good compromise between the required accuracy and the available computational resources.

A Computational details

For the computational details of HSE06, LDA and Hartree calculations of spectral functions in Sec. 3 we refer to Ref.²².

For what concerns the optical spectra of bulk silicon, lithium fluoride and solid argon (see Sec. 4), all calculations have been done with the following procedure: ground-state calculations with Abinit⁸⁴, using plane waves (see Table 1), the local density approximation (LDA)⁸⁵ and Troullier-Martins pseudopotentials⁸⁶; a scissor operator (SO) has been applied to the empty bands to simulate many-body band-gap opening effects (see Table 1); a Bethe-Salpeter calculation constitutes the reference calculation, obtained with the EXC code⁸⁷; the TDDFT calculations with all kernels have been carried out using the DP code⁸⁸. Both BSE and TDDFT spectra results have been evaluated using 7 bands (4 occupied and 3 empty bands) and by sampling the Brillouin zone with 256 inequivalent k-points.

Table 1 Energy cutoff (Ecut) for the ground-state calculations is shown in Hartree. The scissor operator (SO) is shown in eV (like the spectra). The number of G-vectors (G-vec) taken into account in the TDDFT (and BSE) calculations refers to the size of the matrices $P, \chi, \tilde{\chi}$, etc. and gives the amount of crystal local field effects. The number of plane waves (Npw) used to describe the single particle wavefunctions used to construct the χ^0 is also reported.

	Si	LiF	Ar
Ecut	13	40	35
G-vec	59	137	137
Npw	169	561	561
SO	0.8	5.25	6.23

Conflicts of interest

There are no conflicts to declare.

Acknowledgements

Computational time was granted by GENCI (Project No. 544). S.C. would like to acknowledge the support of the Center of Theoretical Physics of Grenoble (CPTG) as well as the hospitality of Laboratoire des Solides Irradiés, École Polytechnique.

Notes and references

- 1 G. Onida, L. Reining and A. Rubio, *Rev. Mod. Phys.*, 2002, **74**, 601–659.
- 2 S. Huotari, in *Spectroscopy in the Frequency Domain*, ed. M. A. Marques, N. T. Maitra, F. M. Nogueira, E. Gross and A. Rubio, Springer Berlin Heidelberg, Berlin, Heidelberg, 2012, pp. 15–28.
- 3 D. Pines, *Elementary Excitations In Solids*, Benjamin, New York, 1963.
- 4 P. Anderson, *Concepts in Solids*, Benjamin, New York, 1963.
- 5 R. M. Martin, L. Reining and D. M. Ceperley, *Interacting Electrons*, Cambridge University Press, 2016.
- 6 A. Damascelli, Z. Hussain and Z.-X. Shen, *Rev. Mod. Phys.*, 2003, **75**, 473–541.
- 7 R. S. Knox, *Theory of Excitons*, Academic Press, 1963.
- 8 F. Bassani and G. P. Parravicini, *Electronic States and Optical Transitions in Solids*, Pergamon Press, 1975.
- 9 P. Elliott, S. Goldson, C. Canahui and N. T. Maitra, *Chemical Physics*, 2011, **391**, 110 – 119.
- 10 K. Sturm and A. Gusarov, *Phys. Rev. B*, 2000, **62**, 16474–16491.
- 11 C. Sternemann, S. Huotari, G. Vankó, M. Volmer, G. Monaco, A. Gusarov, H. Lustfeld, K. Sturm and W. Schülke, *Phys. Rev. Lett.*, 2005, **95**, 157401.
- 12 W. Kohn, *Rev. Mod. Phys.*, 1999, **71**, 1253–1266.
- 13 W. Kohn and L. J. Sham, *Phys. Rev.*, 1965, **140**, A1133–A1138.
- 14 P. Hohenberg and W. Kohn, *Phys. Rev.*, 1964, **136**, B864–B871.
- 15 E. Runge and E. K. U. Gross, *Phys. Rev. Lett.*, 1984, **52**, 997–1000.
- 16 M. Levy, J. P. Perdew and V. Sahni, *Phys. Rev. A*, 1984, **30**, 2745–2748.
- 17 F. Malet and P. Gori-Giorgi, *Phys. Rev. Lett.*, 2012, **109**, 246402.
- 18 A. L. Fetter and J. D. Walecka, *Quantum theory of many-particle systems*, McGraw-Hill, 1971.
- 19 M. Gatti, V. Olevano, L. Reining and I. V. Tokatly, *Phys. Rev. Lett.*, 2007, **99**, 057401.
- 20 A. Ferretti, I. Dabo, M. Cococcioni and N. Marzari, *Phys. Rev. B*, 2014, **89**, 195134.
- 21 M. Vanzini, L. Reining and M. Gatti, *The European Physical Journal B*, 2018, **91**, 192.
- 22 M. Vanzini, L. Reining and M. Gatti, *Dynamical local connector*

- approximation for electron addition and removal spectra, 2017, arXiv1708.02450.
- 23 P. Martin, *Measurements and Correlation Functions*, Gordon and Breach, New York, 1968.
 - 24 A. Georges, G. Kotliar, W. Krauth and M. J. Rozenberg, *Rev. Mod. Phys.*, 1996, **68**, 13–125.
 - 25 L. Hedin, *Phys. Rev.*, 1965, **139**, A796–A823.
 - 26 J. P. Perdew, *Phys. Rev. B*, 1986, **33**, 8822–8824.
 - 27 J. P. Perdew, K. Burke and M. Ernzerhof, *Phys. Rev. Lett.*, 1996, **77**, 3865–3868.
 - 28 J. Tao, J. P. Perdew, V. N. Staroverov and G. E. Scuseria, *Phys. Rev. Lett.*, 2003, **91**, 146401.
 - 29 J. Sun, A. Ruzsinszky and J. P. Perdew, *Phys. Rev. Lett.*, 2015, **115**, 036402.
 - 30 C. Lee, W. Yang and R. G. Parr, *Phys. Rev. B*, 1988, **37**, 785–789.
 - 31 A. D. Becke, *Phys. Rev. A*, 1988, **38**, 3098–3100.
 - 32 A. D. Becke, *The Journal of Chemical Physics*, 1993, **98**, 5648–5652.
 - 33 A. D. Becke, *The Journal of Chemical Physics*, 1996, **104**, 1040–1046.
 - 34 T. W. Keal and D. J. Tozer, *The Journal of Chemical Physics*, 2004, **121**, 5654.
 - 35 Y. Zhao and D. G. Truhlar, *The Journal of Chemical Physics*, 2006, **125**, 194101.
 - 36 D. M. Ceperley and B. J. Alder, *Phys. Rev. Lett.*, 1980, **45**, 566–569.
 - 37 M. Vanzini, A. Aouina, M. Panholzer, M. Gatti and L. Reining, *Recycling knowledge to explore materials: a connector theory approach*, 2019, arXiv1903.07930.
 - 38 L. J. Sham and M. Schlüter, *Phys. Rev. Lett.*, 1983, **51**, 1888–1891.
 - 39 L. J. Sham, *Phys. Rev. B*, 1985, **32**, 3876–3882.
 - 40 R. T. Sharp and G. K. Horton, *Phys. Rev.*, 1953, **90**, 317–317.
 - 41 L. Reining, V. Olevano, A. Rubio and G. Onida, *Phys. Rev. Lett.*, 2002, **88**, 066404.
 - 42 F. Sottile, V. Olevano and L. Reining, *Phys. Rev. Lett.*, 2003, **91**, 056402.
 - 43 G. Adragna, R. Del Sole and A. Marini, *Phys. Rev. B*, 2003, **68**, 165108.
 - 44 A. Marini, R. Del Sole and A. Rubio, *Phys. Rev. Lett.*, 2003, **91**, 256402.
 - 45 R. Stubner, I. V. Tokatly and O. Pankratov, *Phys. Rev. B*, 2004, **70**, 245119.
 - 46 F. Bruneval, F. Sottile, V. Olevano, R. Del Sole and L. Reining, *Phys. Rev. Lett.*, 2005, **94**, 186402.
 - 47 S. Hüfner, *Photoelectron Spectroscopy: Principles and Applications*, Springer, Berlin, 2003.
 - 48 L. Hedin, J. Michiels and J. Inglesfield, *Phys. Rev. B*, 1998, **58**, 15565–15582.
 - 49 J. P. Perdew, R. G. Parr, M. Levy and J. L. Balduz, *Phys. Rev. Lett.*, 1982, **49**, 1691–1694.
 - 50 J. Heyd, G. E. Scuseria and M. Ernzerhof, *The Journal of Chemical Physics*, 2003, **118**, 8207–8215.
 - 51 J. Heyd, G. E. Scuseria and M. Ernzerhof, *The Journal of Chemical Physics*, 2006, **124**, 219906.
 - 52 A. V. Krukau, O. A. Vydrov, A. F. Izmaylov and G. E. Scuseria, *The Journal of Chemical Physics*, 2006, **125**, 224106.
 - 53 J. Paier, M. Marsman, K. Hummer, G. Kresse, I. C. Gerber and J. G. Ángyán, *The Journal of Chemical Physics*, 2006, **124**, 154709.
 - 54 J. Paier, M. Marsman, K. Hummer, G. Kresse, I. C. Gerber and J. G. Ángyán, *The Journal of Chemical Physics*, 2006, **125**, 249901.
 - 55 J. Paier, M. Marsman and G. Kresse, *The Journal of Chemical Physics*, 2007, **127**, 024103.
 - 56 G. D. Mahan, *Many-particle physics*, Plenum Press, New York, 1981.
 - 57 M. Petersilka, U. J. Gossmann and E. K. U. Gross, *Phys. Rev. Lett.*, 1996, **76**, 1212–1215.
 - 58 D. Bohm and D. Pines, *Phys. Rev.*, 1953, **92**, 609–625.
 - 59 S. Botti, A. Schindlmayr, R. D. Sole and L. Reining, *Reports on Progress in Physics*, 2007, **70**, 357–407.
 - 60 E. E. Salpeter and H. A. Bethe, *Phys. Rev.*, 1951, **84**, 1232–1242.
 - 61 G. Strinati, *La Rivista del Nuovo Cimento*, 1988, **11**, 1–86.
 - 62 G. Onida, L. Reining, R. W. Godby, R. Del Sole and W. Andreoni, *Phys. Rev. Lett.*, 1995, **75**, 818–821.
 - 63 S. Albrecht, L. Reining, R. Del Sole and G. Onida, *Phys. Rev. Lett.*, 1998, **80**, 4510–4513.
 - 64 L. X. Benedict, E. L. Shirley and R. B. Bohn, *Phys. Rev. Lett.*, 1998, **80**, 4514.
 - 65 M. Rohlfing and S. G. Louie, *Phys. Rev. Lett.*, 1998, **81**, 2312–2315.
 - 66 E. G. C. P. van Loon, F. Krien and A. A. Katanin, *The Bethe-Salpeter equation at the critical end-point of the Mott transition*, 2020.
 - 67 F. Krien, E. G. C. P. van Loon, M. I. Katsnelson, A. I. Lichtenstein and M. Capone, *Phys. Rev. B*, 2019, **99**, 245128.
 - 68 T. Schäfer, G. Rohringer, O. Gunnarsson, S. Ciuchi, G. Sangiovanni and A. Toschi, *Phys. Rev. Lett.*, 2013, **110**, 246405.
 - 69 T. Schäfer, S. Ciuchi, M. Wallerberger, P. Thunström, O. Gunnarsson, G. Sangiovanni, G. Rohringer and A. Toschi, *Phys. Rev. B*, 2016, **94**, 235108.
 - 70 I. Reshetnyak, M. Gatti, F. Sottile and L. Reining, *Phys. Rev. Research*, 2019, **1**, 032010.
 - 71 R. Del Sole, G. Adragna, V. Olevano and L. Reining, *Phys. Rev. B*, 2003, **67**, 045207.
 - 72 S. Baroni and R. Resta, *Phys. Rev. B*, 1986, **33**, 7017–7021.
 - 73 P. Ghosez, X. Gonze and R. W. Godby, *Phys. Rev. B*, 1997, **56**, 12811–12817.
 - 74 S. Botti, A. Fourreau, F. m. c. Nguyen, Y.-O. Renault, F. Sottile and L. Reining, *Phys. Rev. B*, 2005, **72**, 125203.
 - 75 S. Botti, F. Sottile, N. Vast, V. Olevano, L. Reining, H.-C. Weissker, A. Rubio, G. Onida, R. Del Sole and R. W. Godby, *Phys. Rev. B*, 2004, **69**, 155112.
 - 76 S. Sharma, J. K. Dewhurst, A. Sanna and E. K. U. Gross, *Phys.*

- Rev. Lett.*, 2011, **107**, 186401.
- 77 S. Rigamonti, S. Botti, V. Veniard, C. Draxl, L. Reining and F. Sottile, *Phys. Rev. Lett.*, 2015, **114**, 146402.
- 78 Y.-M. Byun and C. A. Ullrich, *Phys. Rev. B*, 2017, **95**, 205136.
- 79 J. E. Rowe and D. E. Aspnes, *Phys. Rev. Lett.*, 1970, **25**, 162–165.
- 80 R. M. Martin, J. A. Van Vechten, J. E. Rowe and D. E. Aspnes, *Phys. Rev. B*, 1972, **6**, 2500–2502.
- 81 F. Sottile, K. Karlsson, L. Reining and F. Aryasetiawan, *Phys. Rev. B*, 2003, **68**, 205112.
- 82 G. Giuliani and G. Vignale, *Quantum theory of the electron liquid*, Cambridge University Press, 2005.
- 83 E. K. U. Gross and N. T. Maitra, in *Introduction to TDDFT*, ed. M. A. Marques, N. T. Maitra, F. M. Nogueira, E. Gross and A. Rubio, Springer Berlin Heidelberg, Berlin, Heidelberg, 2012, p. 53.
- 84 X. Gonze, G.-M. Rignanese, M. Verstraete, J.-M. Beuken, Y. Pouillon, R. Caracas, F. Jollet, M. Torrent, G. Zerah, M. Mikami *et al.*, *Z. Kristallogr.*, 2005, **220**, 558–562.
- 85 J. P. Perdew and Y. Wang, *Phys. Rev. B*, 1992, **45**, 13244–13249.
- 86 N. Troullier and J. L. Martins, *Phys. Rev. B*, 1991, **43**, 1993–2006.
- 87 L. Reining, V. Olevano, S. Albrecht, G. Onida and F. Sottile, unpublished.
- 88 V. Olevano, L. Reining and F. Sottile, The DP code, unpublished.